Article

Jupiter revealed as a real (high-power) pulsar: magnetar- & dwarf novae-type prebursting evolution of Jovian global magnetoactivity since 1996

Mensur Omerbashich

Geophysics Online, Los Angeles, CA 90250, https://orcid.org/0000-0003-1823-4721
Correspondence: omerbashich@geophysics.online, editor@geophysicsjournal.com

Abstract: The decade-scale magnetoactivity evolution profile preceding short-burst pulses — observed in magnetar 4U 0142+61, and superhumps (superoutbursts) — in dwarf novae, emerged from mean least-squares spectra of mission-integrated Galileo–Cassini–Juno 1996–2020 annual samplings of Jupiter $\lessgtr$8nT global magnetic field. The profile revealed for the first time the pulsar nature of Jupiters by temporally mapping hyperlow-frequency (<1μHz) systematic dynamics of the magnetospheric signature in the solar wind (Rieger-resonance band of 385.8–64.3 nHz, or ~0.3·10^9–3·10^9 erg energetic perturbations) used as a proxy of Jovian magnetoactivity expressed in mean least-squares spectral magnitudes as a novel method for measuring relative field dynamics. The magnetoactivity impressed into the solar wind entirely, encompassing the well-known and Solar system-permeating ~154-day Rieger period and its first six harmonics. Statistical fidelity of spectral peaks stayed well within a very high (Φ≫12) range, 10^7–10^5, reflecting the signature's completeness and incessantness. The magnetoactivity upsurge from spectral means that maintained a stunning ~20% field variance (total energy budget) began reformatting the signature around 1999, gradually transforming it into the anomalous state by 2002, as supported by an increased anisotropic splitting of spectral peaks. In contrast, a comparison against 2005–2016 Cassini global samplings revealed a calm Saturnian magnetoactivity at a low $\lessgtr$1% field variance except for every ~7.1 yrs., when it is $\lessgtr$5% due possibly to orbital–tidal forcing. The discovery of a global pulsation profile of magnetar–novae type in a planet demands beacon-orbiter missions to monitor Jupiter's magnetoactivity and its disruption capacity, if any, to Solar-system infrastructure.

Keywords: *Jupiter; Saturn; magnetospheric activity; planetary magnetospheres–solar wind interaction; pulsars; pulsar outbursts*

Highlights

- First mission-integrated study of Jovian global magnetic activity over decadal scales and using all Jupiter & Saturn *in situ* data
- Expanded early claims on Jupiter resembling a (low-power) pulsar by conclusively showing it is a real (high-power) pulsar
- Discovery revealed the exact manner in which Jupiters jump between the star and planet states
- The jump is moderated by a gradually varying sinusoidal energy dissipation regime observed in magnetars & dwarf novae
- The regime represents a part of the confirmed pre-outbursting sequence, calls for a permanent monitoring mission at Jupiter
- First application of rigorous Gauss-Vaniček Spectral Analysis (GVSA) by least squares in global planetary physics
- GVSA revolutionizes space physics by rigorously simulating completed orbits & fleet formations from a single spacecraft.

1. Introduction

Global macroscopic fields, including magnetic, electric, and gravitational–rotational, interact mutually in astronomical bodies to create dynamic systems with varying degrees of complexity. Then the intricate random, chaotic, systematic, and periodic dynamical systems engage in feedback activity individually with those fields. For example, the interaction of planetary magnetic fields and planetary dynamics includes the dynamo mechanism of the core's and fluids' kinetic→electric→magnetic energies conversions, overall core-surface processes, and the generation of atmospheric electric currents, including ionospheric ones; see, e.g., Matsushita (1967).

Jupiter's intricacies stand out in many ways in our solar system. These include a magnetic field different from all other known planetary magnetic fields (Moore et al., 2018), whose interaction with the solar wind as the builder of planetary magnetospheres has been demonstrated, e.g., by Murakami et al. (2016) from the Hisaki satellite data, yet remains poorly understood (Masters, 2017). To refine our understanding of Jupiter's large-scale dynamics, I employ this proven interaction as a proxy of the Jovian magnetosphere's global dynamics and identify any signatures of decade-scale changes in Jupiter's magnetoactivity (total magnetic field) imprinted onto the solar wind. Here magnetoactivity is represented per epoch of choice (one year) as the mean spectral magnitude of spacecraft magnetometer measurements taken over that epoch. Such representation reflects the known fact that, due to turbulence and unknown reasons, global Jovian dynamics exhibit resonance at all energy scales, so much so that the Jupiter magnetosphere can be treated as an infinite set of independent resonators, each with its own natural frequency and so its own set of harmonics (Wright and Mann, 2013). Then spectrally expressed magnetoactivity describes the overall magnetic excitement of an astronomical object of study like Jupiter. Such average spectral magnitudes from Fourier spectra previously were used to measure decadal levels of magnetoactivity of a magnetar, e.g., Gonzalez et al. (2010), the top-left panel of their Fig. 2. Here, effects of sub-annual planetary magnetic field variations and changing spacecraft orbits were ironed-out globally (maneuvers and moon flybys discarded).

The Rieger resonance (RR) process is amongst the most vigorous systematic global solar wind dynamics. The leading, transient, and well-known Rieger period (Chowdhury et al., 2009), $P_{Rg}=\sim154$-day (~150–160-day), characterizes this process. Rieger et al. (1984) discovered P_{Rg}, whose 5/6 P_{Rg}, 2/3 P_{Rg}, 1/2 P_{Rg}, and 1/3 P_{Rg} harmonics, i.e., ~128, ~102, ~78, and ~51-day periods, were subsequently reported in numerous studies and from different kinds of data, and are called the Rieger-type periodicities (Dimitropoulou et al., 2008). P_{Rg} originates in the Sun and is the guiding period of the solar wind in the highest planetary energies, resulting in its power and prominence on macroscopic scales (Omerbashich, 2023a; 2023b). P_{Rg} equates to 154 days most of the time, so $2P_{Rg}$ equates to the 1-yr window of the epoch of choice transiently rarely, if ever. Thus P_{Rg} is characterized by its transient nature and the fact that it is not always the strongest or longest; instead, power gets shared amongst harmonics. These circumstances enable, i.e., do not prevent, using the entire RR band indiscriminately, or using the average spectra in that band as a measure of global magnetoactivity. Namely, since P_{Rg} most of the time is the most prominent period of RR, P_{Rg} relates to the epoch's (one-year-spanning) window most of the time by a factor of $2 \cdot 154/365=0.8$, a value commonly regarded as safe in terms of alleviating main problems including spectral leakages. Finally, the spectral analysis method used in the present study does not depend on the Nyquist frequency (Craymer, 1998).

A damped, periodically forced nonlinear oscillator, which exhibits both periodic and chaotic behavior, successfully simulates RR (Bai and Cliver, 1990). The Rieger period was confirmed in solar flares rates (Kiplinger et al., 1984) and reported in the interplanetary magnetic field (IMF) (Cane et al., 1998) and most heliophysics data types: photospheric magnetic flux, group sunspot numbers, proton speed, and others; see, e.g., Carbonell and Ballester (1992) for a summary of such reports. Namely, we know that the Sun is a body whose vibrations, polarity, and alternate current (AC) propagate via emitted solar wind into the heliosphere (the zone of the Sun's macroscopic influence, up to ~50–100 AU beyond Pluto orbit). As a composite of mechanical carrier waves transporting those remnants and features, the wind's own magnetism forms what we refer to as IMF. While the Jovian magnetic field is internally-generated (Manners and Masters, 2020), the solar wind dominantly shapes the magnetic fields of all magnetized bodies in the solar system into congruent bubbles of magnetism called magnetospheres. Therefore, the energy band of RR, where this main (most energetic) planet–star action by the solar wind occurs, is the band of interest in the present study. The Rieger *band* (not P_{Rg}) is an intermediary or the common grounds that enables us to draw a link between the two energy scales: hourly, of

main (rotational) interactions, and decadal, encompassing decadal global dynamics of an entire astronomical body.

To examine the criticality of RR for Jovian magnetodynamics, I use all available data from space missions that orbited or flew by Jupiter for six months or more. I then temporally map the annual effects of the Jovian magnetosphere onto the surrounding solar wind as represented by the band of its inherent RR process. To measure the change in magnetoactivity, I employ a method for measuring field dynamics by Omerbashich (2009, 2007, 2003). As mentioned, to isolate any signatures of Jovian decade-scale global magnetoactivity in the solar wind — the RR band in particular — requires ignoring the effects of any Jovian satellites, flybys of which then get omitted from the analyses. This data removal is justified because the analysis method employed in the present study is the only rigorous spectral analysis method unaffected by gaps in raw data.

2. Data and methodology

To temporally map hyperlow-frequency (<1μHz) dynamics in the solar wind near Jupiter, I spectrally analyze magnetometer recordings collected between 1996 and 2020 in Jupiter and, for a check, Saturn vicinity in the 1–6-month (30–180-day) band of RR. Because the Sun-outward direction is critical to correctly mapping the dynamics of a solar system-wide process, and I study the two gaseous giants Jupiter and Saturn globally, a coordinate system independent of both planets is required. Thus I use the Sun RTN (Radial–Tangential–Normal) as the optimal Space coordinate frame for the present study. The RTN coordinate system, or the Spacecraft–Solar equatorial (SE) system, consists of a Normal component, B_N, roughly normal to the solar equatorial plane, a Tangential component, B_T, parallel to the solar equatorial plane, a Radial component B_R, which points in the Sun–spacecraft direction outwards from the Sun, and Total (average) field, B, obtained from the field components in the usual way. This choice preserves the relative orientation of the magnetopause–wind collision interface to always point toward the Sun. In that context, the Rieger mechanical resonant process RR in IMF is, for simplicity, taken as particles of solar ejecta that blanket the ecliptic and flap resonantly about it. The Galileo data included full-year magnetometer recordings at Jupiter from 1996–2002 inclusively; the Juno data included full-year recordings at Jupiter from 2017–2020 inclusively; full-year Cassini recordings at Saturn spanned 2005–2016 inclusively, while the 1 September 2000–31 April 2001 recordings covered the October 2000–March 2001 Jupiter flyby by Cassini. Note here that, due to significant dissimilarities in their physical properties, chemical composition, and field strengths, only the existence and mode of change in Jupiter's vs. Saturn's global magnetoactivity over the same few decades is comparable, but not their dynamics individually for any given year. To expedite the computation, I decimate the data, i.e., take 100-minute averages of magnetometer recordings to represent the field with a realism sufficient given the band of interest.

The Galileo and Juno data were provided to me concatenated and rotated to RTN (Sun) coordinate frame (see Acknowledgments). The Cassini data used were the updated and calibrated 1-minute averages v2.0 of Cassini magnetometer recordings spanning 2000–2017 (2000.01.20:18:28:30–2017.09.12:15:14:31), where the portion preceding 01 January 2001 used an older calibration (Dougherty et al., 2006).

For simplicity, I assume Jupiter's magnetosphere acted alone on the nearby solar wind. Then the solar wind is the sole systematic dynamic impressed onto the magnetosphere. I tacitly adopt that incidental processes, including substorm-like events caused by internal processes such as mass loading of iogenic plasma (Ge et al., 2007) (Tsuchiya et al., 2018), have little relevance for the present study that is concerned with systematic periodic global dynamics primarily. At the same time, and owing to Jupiter's size, yearlong data sampling presumably makes the variation in spacecraft distance to observed field features

like central plasma sheet irrelevant. Furthermore, effects from all fields, including magnetospheric components and background noise, can be expected to cancel out under planetary rotation, e.g., Gaulme et al. (2011). This scenario is plausible also because only the highest interplanetary solar-wind energies (~0.2–2 ZeV or ~0.3·10⁹ –3·10⁹ erg) are of interest here, making the sampled magnetoactivity variation virtually radial. This scenario is also the optimal way to properly account for variability features in the Jupiter predominantly radial field; see Moore et al. (2018). Besides, I discard maneuvers and flybys of other celestial bodies to constrain the maximum field strengths used to the ~4 to ~8 nT interval as Jupiter's natural range of highest field strengths. For instance, since the field-component observations taken when Juno was relatively far from the central plasma sheet were ~8 nT vs. ~1 to 4 nT (Yao et al., 2021), and the magnetosphere–IMF interaction at Jupiter is poorly understood, I use the middle field and iron out effects of spacecraft varying orbit on the measurements of field strength. This approach added rigor to the analysis.

The magnetometer data show occasional inexplicable swellings (Steven Joy, personal communication, 2021; ref. Acknowledgments) that exceed the declared data precision in the product-delivered values of total magnetic field observations, as obtained from theoretical vs. complete observed component values. I confirmed the same on random samples supplied to me (see Acknowledgments) for 2009, 2011, and 2014. Therefore, to retain strictness and uniformity in an analysis that relies on a mission integration, I compute commonly used theoretical (average) total magnetic field strength values from the product field components throughout and for all missions in the usual way, as $B = \sqrt{B_R{}^2 + B_T{}^2 + B_N{}^2}$ for each magnetometer measurement of the three components (R, T, N) of the magnetic field.
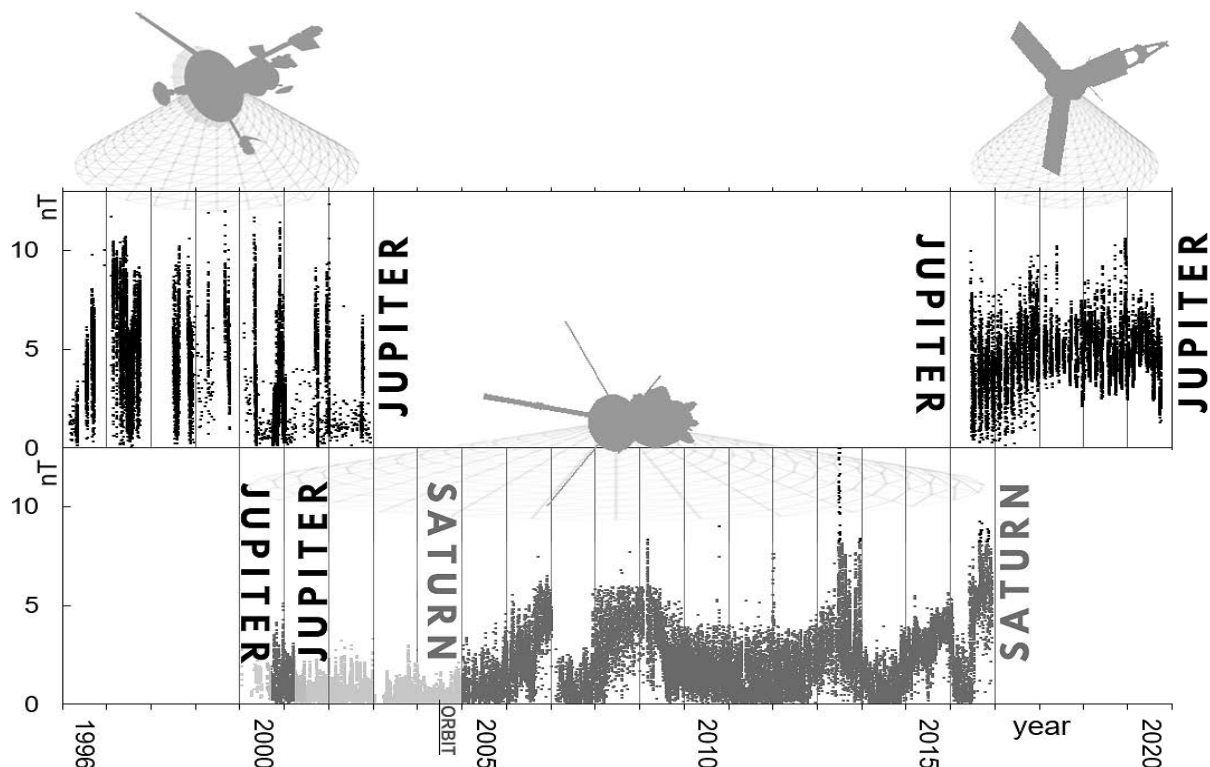
Figure 1. Plots of Jupiter and Saturn magnetic field data analyzed 100-minute-decimated averages. Top panel — Jupiter magnetometer data after removing maneuvers and flybys of natural satellites and other planets, from Galileo mission between 29 March 1996–11 November 2002 (left-hand side), and Juno mission between 07 July 2016–09 September 2020 (right-hand side). Bottom panel — Saturn magnetometer data after removing maneuvers and flybys of natural satellites and other planets except for 03 October 2000–31 March 2001 Jupiter flyby data (left-hand side), from Cassini mission between 01 January 2005–31 December 2016 (right-hand side). Used datasets are continuous gapped time series that, in all cases, comprised at least half-a-year-spanning samples on data sets' ends and whole-year-spanning samples from each Earth calendar year in which any of the three missions flew by either Jupiter or Saturn. Note the Cassini orbit insertion at Saturn, of 01 July 2004. The data are in the Supplement; see statements.
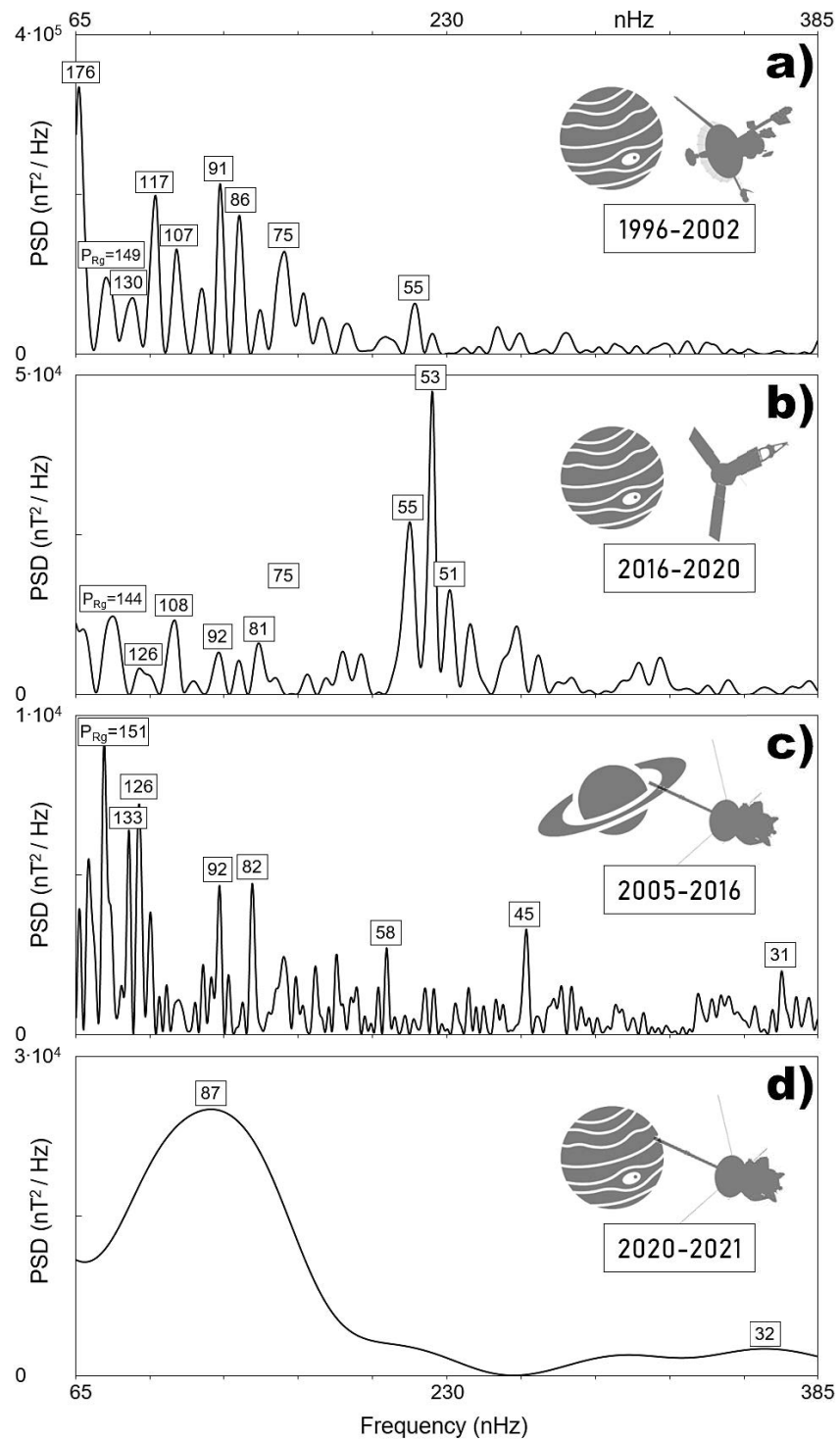
Figure 2. Plots of power spectral density (PSD), in nT²/Hz, for Galileo magnetometer recordings of the Jupiter magnetic field, 1996–2002 (panel a), Juno recordings of the Jupiter magnetic field, 2016–2020 (b), Cassini recordings of the Saturn magnetic field, 2005–2016 (c), and Cassini recordings of the Jupiter magnetic field, 2000–2001 (d). Labels on spectral peaks show periods in days. The frequency spectral band of 65–385 nHz corresponds to the Rieger process's 30–180-day band (band of interest in the present study).

As seen from Fig. 2, panels a–c, although unstable due to their transient nature, the Rieger period, P_{Rg}, and its harmonics (Rieger-type periodicities, Dimitropoulou et al., 2008), are nonetheless present in the overall data, Fig. 1. Thus the 100-minute-decimating preserved data quality while not introducing any artificial systematic processes. Looking at the Galileo and Juno samplings of Jupiter (going from panels a to b via d), the Jovian magnetic field progressively impeded RR in the solar wind, first (Galileo, panel a) by allowing lower Sun harmonics like the 176-day to take up the power. Then, by the time of Juno mission samplings of Jupiter, panel b, the field has entirely squashed the RR process in the lowermost-frequencies (highest energies) part. Finally, the Saturn magnetic field did not affect RR significantly, panel c. In addition, the above conclusions are not affected by solar cycle maxima that enhance P_{Rg}. Namely, Galileo samplings of Jupiter, panel a, and Cassini samplings of Saturn, panel c, were taken during one solar cycle maximum each and towards the end of the sampling time interval — the solar cycles 23 and 24, respectively. The relatively brief, 6-month flyby of Jupiter by Cassini, panel d, was perhaps also impeded by Jupiter's magnetoactivity increase (of sinusoidal dissipation), seen as the resonance power shuffling into a single mid-spectral peak as all the higher harmonics got extinguished. However, the relatively minimal duration of the flyby has also prevented P_{Rg} and lower Sun harmonics from appearing.

Spectra were computed in var% and dB against linear background noise levels using the rigorous Gauss–Vaníček method of spectral analysis (GVSA) by Vaníček (1969, 1971). GVSA is easily programmable, which enables full integration of spectral computation algorithms with complete statistical analysis and testing abilities into a scientific software package. The easy-to-use package, LSSA (Least Squares Spectral Analysis), provides periodicity estimates in the strictly least-squares sense, unlike the more popular Lomb-Scargle approximation of GVSA. Zhou and Sornette (2002) exposed the ineptness of the Fourier and Lomb-Scargle techniques for extracting periodicities in turbulent or generally colored data and for attaching a significance level to such periodicities when the nature of the noise is unknown. GVSA, on the other hand, with its statistical-physical (absolute) significance level regime, alleviates these problems, enabling the separation of real from spurious harmonics generally (Omerbashich, 2023c) and not only when a resonance process is expected, like in the present study. GVSA has many benefits and advantages over Fourier methods (Omerbashich, 2021, 2007, 2006; Press et al., 2007; Pagiatakis, 1999; Wells et al., 1985; Taylor and Hamilton, 1972). Besides, the conventional Fourier transform and spectrum are just special cases of more general least-squares formulations (Craymer, 1998). GVSA revolutionizes physics by enabling direct computations of nonlinear dynamics, rendering classical approaches such as spherical approximation obsolete (Omerbashich, 2023a).

To arrive at the main result, I do not use spectral analysis results in the classical sense, i.e., periods and frequencies, but primarily mean spectral magnitudes. The means are taken over the spectral band of interest and obtained from annual subsets of all the available data needed for the present study, where one Earth year is the epoch of choice. (Note again that GVSA is the only rigorous spectral analysis method impervious to data incompleteness and the Nyquist frequency phenomenon when analyzing unevenly spaced data.) In classical approaches, ratios of Fourier spectral amplitudes of some dynamic get compared in between to learn about a field's relative activity. However, Omerbashich (2009, 2007, 2003) has developed a method for measuring field dynamics, in which the mean variance-spectrum (average variance-spectral magnitude) over the spectral band of interest represents field dynamics, i.e., change in system energy dissipation levels over the corresponding data span (epoch of interest). This representation is enabled primarily by the linear expression of background spectral noise in GVSA.

In its simplest form, i.e., when there is no *a priori* knowledge on data constituents such as datum offsets, linear trends, and instrumental drifts, a GVSA spectrum s is computed for n=1000 corresponding periods T_j or frequencies ω_j and output with spectral magnitudes M_j, as (Omerbashich, 2004):

$$s_j(T_j, M_j) = \boldsymbol{s}(\omega_j, M_j) = \frac{\boldsymbol{l}^{\mathrm{T}} \cdot \boldsymbol{p}(\omega_j)}{\boldsymbol{l}^{\mathrm{T}} \cdot \boldsymbol{l}}, j = 1 \dots n \ \wedge \ j \in \mathbb{Z} \ \wedge \ n \in \aleph, \tag{1}$$

obtained after two orthogonal projections. First, of the vector of m observations, $\boldsymbol{l}$, onto the manifold Z ($\boldsymbol{\Psi}$) spanned by different base functions (columns of $\mathbf{A}$ matrix) at a time instant t, $\boldsymbol{\Psi} = [\cos \omega t, \sin \omega t]$, to obtain the best fitting approximant $\boldsymbol{p} = \sum_{i=1}^m \hat{c}_i \, \boldsymbol{\Psi}_i$ to $\boldsymbol{l}$ such that the residuals $\hat{\boldsymbol{v}} = \boldsymbol{l} - \boldsymbol{p}$ are minimized in the least-squares sense for $\hat{\boldsymbol{c}} = (\boldsymbol{\Psi}^{\mathrm{T}} \mathbf{C}_l^{-1} \boldsymbol{\Psi})^{-1} \cdot \boldsymbol{\Psi}^{\mathrm{T}} \mathbf{C}_l^{-1} \boldsymbol{l}$. The second projection, of $\boldsymbol{p}$ onto $\boldsymbol{l}$, enables us to obtain the spectral value, Eq. (1). Vectors $\boldsymbol{u}_j = \boldsymbol{\Psi}^{\mathrm{T}} \, \boldsymbol{\Psi}_{NK+1}$ and $\boldsymbol{v}_j = \boldsymbol{\Psi}^{\mathrm{T}} \, \boldsymbol{\Psi}_{NK+2}$, j=1, 2…. NK$\in\aleph$, compose columns of the matrix $\mathbf{A}_{NK,NK} = \boldsymbol{\Psi}^{\mathrm{T}} \, \boldsymbol{\Psi}$. Note here that the vectors of known constituents compose matrix $\hat{\mathbf{A}}_{\mathrm{m,m}} = \hat{\boldsymbol{\Psi}}^{\mathrm{T}} \, \hat{\boldsymbol{\Psi}}$, in which case the base functions that span the manifold $Z(\boldsymbol{\Psi})$ get expanded by known-constituent base functions, $\hat{\boldsymbol{\Psi}}$, to $\boldsymbol{\Psi} = \left[\hat{\boldsymbol{\Psi}}, \cos \omega t, \sin \omega t\right]$. For a detailed treatment of GVSA with known data constituents, see, e.g., Wells et al. (1985). Subsequently, the method got simplified into non-rigorous (strictly non-least-squares) formats like the above-mentioned Lomb-Scargle technique created to lower the computational burden of the Vaníček's pioneering development, but which no longer is an issue.

GVSA is strict in that, besides estimating a uniform spectrum-wide statistical significance in var% for the desired level, say 95%, in a spectrum from a time series with m data values and q known constituents as $1-0.95^{2/(m-q-2)}$ (Steeves, 1981) (Wells et al., 1985), it also imposes an additional constraint for determining the validity of each significant peak individually — the fidelity or realism, Φ. In advanced statistics, fidelity is a general information measure based on the coordinate-independent cumulative distribution and critical yet previously neglected symmetry considerations (Kinkhabwala, 2013). In communications theory, fidelity measures how undesirable it is (according to some fidelity criterion we devise) to receive one piece of information when another is transmitted (Shannon, 1948). In GVSA, fidelity thus is defined in terms of the theory of spectral analysis as a measure of how undesirable it is for two frequencies to coincide (occupy the same frequency space of a sample). A value of GVSA fidelity is obtained then as that time interval (in units of the timescale of the time series analyzed) by which the period of a significant spectral peak must be elongated or shortened to be π-phase-shiftable within the length of that time series. As such, Φ measures the unresolvedness between two consecutive significant spectral peaks (those that cannot be π-phase-shifted). When periods of such spectral peaks differ by more than the fidelity value of the former, those peaks are resolvable. As the *degree of a peak's dependence by the tendency to cluster*, this criterion reveals whether a spectral peak can share a systematic nature with another spectral peak, e.g., be part of a batch, or be an underlying dynamical process like resonance or reflection. Spectral peaks that meet this criterion are in the LSSA software output listed amongst insignificant, and the rest amongst significant (hereafter: *physically-statistically significant peaks* or just (fully) *significant peaks* for short).

Omerbashich (2006) then empirically deduced an additional criterion of stringency: that GVSA fidelity in prominently periodic time series (with more than just a few periodicities) to reasonable approximation satisfies a Φ>12 common criterion for the individually genuine significance of a systematic process and therefore most of its periodicities as well. Thus, spectral peaks with a declared fidelity value below this threshold are readily dismissible as noise also (except for re-emitted systematic processes like resonance overtones and undertones). Consequently, in a prominently periodic time series, an abundance of spectral peaks with a stated fidelity value indicates a systematic process with mutually dependent spectral constituents if most of the computed or theoretical (say, all or most of the supposed harmonic) spectral peaks of interest meet the threshold. Inversely, predominant independence of spectral peaks (when Φ<12 mostly holds) is encountered rarely in time series describing real dynamical and quasiperiodic processes in physical

sciences and generally naturally repetitive (systematic) processes in abstract disciplines. But if a time series has spectral peaks with both $\Phi > 12$ and $\Phi < 12$ to a roughly equal measure, periods mostly are independent or dynamics-unrelated (the "noise" when suspecting a systematic process) regardless of their statistical significance. Particularly so at a low statistical significance level (67% in absolute terms, unless constrained by additional criteria or data dependencies). So a prominently periodic time series characterized by $\Phi \gg 12$ describes a systematic process practically certainly, and in cases of detecting widely reported physical processes such as natural resonances, certainly. The above-listed abilities make GVSA a desired technique for detecting systematic (harmonic) and quasiperiodic events and system processes like resonances, antiresonances, and reflections.

In addition, Omerbashich (2021, 2020) computationally empirically established a *relative fidelity* criterion, according to which spectral peaks with fidelity within ~order-of-magnitude away from the resonance mode (driver) period's fidelity usually share (or not) physical relevancy with the driver and can in this way as well be identified as belonging to a systematic process (or not). This order-of-magnitude internal dependency amongst peaks with their fidelity declared ("super-significant peaks") is mainly due to the above-mentioned linear background representation of spectral magnitudes and related quality of a GVSA spectrum as a variance-based (therefore a most natural) descriptor of relative field dynamics, i.e., energy subbands and budgets (Omerbashich, 2003, 2007, 2009). Here the overall sensitivity of GVSA fidelity to energy-band variations within a physical system is not analysis-driven. So when a resonance process features mostly $\Phi \gg 12$ peaks, the spectral peaks of its overtone process could attain a mostly $\Phi \ll 12$ range and still be physically meaningful by belonging to some $\Phi \gg 12$ process(es). Generally, GVSA fidelity values in a prominently periodic time series of real data respond congruently to physical situations varying in statistical and physical parameters. This sturdiness reveals a genuinely separate meaning to the GVSA fidelity as a unified (physical–statistical) parameter that approximates reality qualitatively better than any distribution-confined statistical parameter(s). For example, the above-noted riddance (of the tendency of spectral peaks to cluster for any reason other than (mostly) physical) alone makes GVSA the preferred method for detecting and modeling peak-splitting anisotropy in data, which is the primary reason for using Φ criteria in the present study. Essentially, the $\Phi > 12$ is an empirical (ad hoc) physical criterion but one that is remarkably natural.

As mentioned above, by discarding variations that spacecraft maneuvering and flyby events left in the record, I also take advantage of the blindness to data gaps as a feature exclusive to the least-squares class of spectral analysis techniques. This advantage is extendable further after data purification — to separate data into portions when the spacecraft sampled a specified body or field of interest alone. Then all such data segments pertinent to the same astronomical body can be patched together, i.e., as though the spacecraft was constantly scanning that object of interest, from the start timestamp of the first to the end timestamp of the last segment. Moreover, combined statistical-physical significance regimes in GVSA enable a realistic piecewise treatment of spacecraft orbits. Thus discarding data collected during unwanted flybys, maneuvers like orbit insertion, and time intervals in which the spacecraft was not operational makes it possible for remaining segments of the record to describe orbital traversals perfectly — as though achieved constantly without interruption, effectively simulating multiple simultaneously operating spacecraft of identical performance.

Magnetoactivity, $^{magnet.}\Lambda$, of an astronomical body in the present study is the instantaneous signature (reduced to an epoch value) of that body's magnetic field strength impressed onto the solar wind in the 30–180-day band of the wind's most vigorous dynamics (at and around RR) during an epoch of choice, here one Earth year. Then change of magnetoactivity with time (the magnetoactivity profile; the profile) is represented by a discrete temporal function $^{magnet.}\Lambda$ containing epoch–to–epoch-consecutive values of the mean spectral magnitude from the spectrum of spacecraft's magnetometer recordings taken over the respective epoch, up to $k=24$ epochs in total. Of those 24 epochs, 13 were during

the Galileo and Juno orbiting stages at Jupiter (including one overlapping instance, by Cassini) and 12 during the Cassini orbiting stage at Saturn, Fig. 1. The (simple) averaging is done over all spectral frequencies in the GVSA spectrum s with the resolution set at n=1000 spectral points or frequencies, obtained using Eq. (1):

$$s_j^{\mathrm{GV}}\left(\omega_j, \mathrm{M}_j^{\mathrm{GV}}\right) \qquad (2)$$

as

$$^{\mathrm{magnet.}}\Lambda_i = \frac{1}{n}\sum_{j=1}^{n} s_j^{\mathrm{GV}}\Bigg|_i \; ; \; i = 1 \dots k \;\; \wedge \;\; k \in \aleph, \qquad (3)$$

so that

$$^{\mathrm{magnet.}}\boldsymbol{\Lambda} = \left\{ ^{\mathrm{magnet.}}\Lambda_1, \; ^{\mathrm{magnet.}}\Lambda_2 \dots, \; ^{\mathrm{magnet.}}\Lambda_k \right\}. \qquad (4)$$

Since spectral magnitudes in var% are proportional to energy levels in dynamical systems, magnetoactivity as a descriptor of change in field dynamics and expressed in var% takes values proportionate to energy fluctuations that arise due to resonant absorption or magnification. Since, due to missing years, the degree to which the energy dissipation is sinusoidal (or not) cannot be represented mathematically, say with the Abbe number $\mathcal{A}$ (von Neumann, 1941), we rely on visual inspection. The higher the value of a spectral magnitude in var%, the higher the sinusoidal global dynamics profile in dominantly rotating bodies, including gaseous giants like Jupiter and Saturn, or pulsating stars like magnetars. Inversely: any significant decade-level divergence from/into the sinusoidal form of a body's dynamics profile indicates the system's overall (global) instability. When a global (here intrinsic) magnetic field turns out to be tracing the said profile, Eq. (4), as in the present study, such divergence could reveal the controlling mechanism that drives that system between its extreme states. In such cases, the driving can be either external, as due to other bodies, or internal, due to the cumulative effect of resonance magnification in one or more internal field dynamics.

3. Results

That the Jupiter magnetosphere was in the above way indeed sampled largely radially, and data treatment and processing approach were correct, can be seen from Fig. 3(a) (radial field component) vs. Fig. 3(d)–(e) (total-field) that yielded practically the same result. The same follows from the statistical fidelity Φ that, as estimated by the LSSA package, stayed well within a very high ($\Phi \gg 12$) range of 10^7–10^5 from lowest- to highest-frequency spectral peaks, respectively. Thus, the RR imprint via solar wind onto the magnetopause and downward was complete and incessant for all practical purposes. Note, while the 99%-significance level in all cases was very close to the 67%-level, the latter is considered sufficient for validating widely reported physical period ensembles, as is the case here. Fidelity in the Saturn field spectra was over half an order of magnitude below the Jupiter field spectra, in the $3.7 \cdot 10^6$–10^5 range. Since the present study does not rely on any period or frequency extraction, and all the noise effects expectedly cancel out over decades under rotation and radial stratification, the mean-field variance values have no assigned uncertainties other than the generic ±5%. As already mentioned, the magnitude space of field variances as a measure of field relative dynamics/system energy dissipation change is the space of interest rather than the frequency space used classically in spectral analysis studies. Therefore, the strictly established statistical–physical significance positively identifying the presence of RR suffices for establishing the credibility of (mean) field variance values. (In terms of statistics: the statistical significance of an extracted but previously known physical process is 100%).

As seen in Fig. 3(e), variation in the upsurge's mean-spectral amplitude from annual-epoch magnetometer records is becoming more sinusoidal with time. This mode of system energy dissipation resembles the evolution of magnetoactivity before short-burst pulses in 4U 0142+61 magnetar, whose decade-long profile of magnetoactivity from the highest-resolution data available (top-left panel of Fig. 2 by Gonzalez et al., 2010) is comparable to that of Jupiter. This dissipation mode was also previously reported in dwarf novae before superoutbursting (Kuznetsova et al., 1999). Note that incomplete (closer to half-year) epochs for the Cassini-2001/2002 and Juno-2016 data, while sufficient for estimating average magnetoactivity per epoch, Eqs. (3)–(4), still lacked information for a detailed depiction of anisotropy. Ironing out the field by discarding measurements taken during maneuvers and flybys of other celestial bodies has resulted in band-wide-mean variance-spectral magnitudes exposing the relative magnetoactivity more successfully in terms of detailed features than can be achieved classically, e.g., by looking into the inherently coarse variation in the anisotropically split spectral peaks. The overall attained levels in the Jupiter decadal global magnetoactivity from the mean spectra, of a staggering ~20% field variance, indicate that an external systematic (lone) signal dominated the band of interest, which, in turn, justified initial assumptions on the solar wind being the sole actor in the Jovian $\sim 0.3 \cdot 10^9$–$3 \cdot 10^9$ erg domain. The main result, namely the demonstrated increase (of sinusoidal dissipation) in the Jupiter magnetoactivity Fig. 3, is comparable to that seen in Fig. 2(a, b, d), where plots of power spectral density (PSD) in the RR band revealed impediment of this highest-energies dynamic of the solar wind by Jupiter magnetoactivity.

For independent astrophysical verification of the Jupiter result in Fig. 3, I perform the same type of analysis for Saturn using the 2005–2016 Cassini samplings of the Saturnian $\lesssim 8nT$ global magnetic field. Comparison of the Saturn result from Fig. 4. against Fig. 3 reveals that, in contrast to the Jovian magnetoactivity increase, Saturn exhibited no activity above relatively very low (weak) ~1% field variance, other than on two occasions 7.1 years apart when Saturnian magnetoactivity climbed to a low ~5% field variance, possibly due to the Saturn's orbital-tidal forcing, of ~7.3 years or ¼T_{orbit}, where $T_{orbit} \approx 29.4$ years. This result is equivalent to that in Fig. 2(c), where a PSD plot in the RR band indicated that this highest-energies dynamic in the solar wind was probably not affected significantly by any other processes.
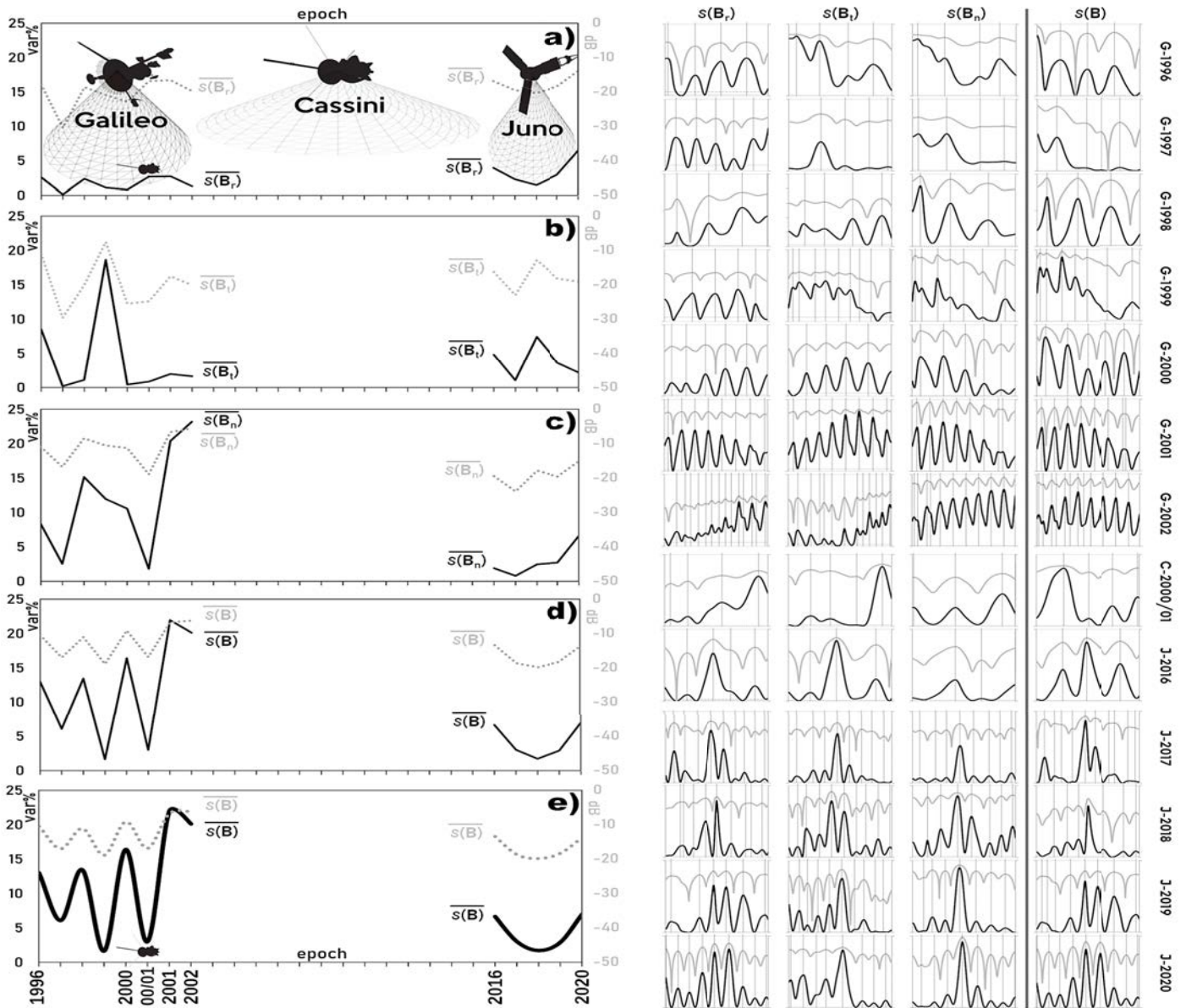
Figure 3. *Left composite*: Decade-scale relative change of Jupiter magnetosphere activity with time as imprinted in the solar wind (interplanetary magnetic field – IMF), as the change in mean GVSA spectral magnitudes in var% (solid black line) and dB (dotted gray) of annual Jovian ≲8nT global magnetic field in the 30–180-day band of most energetic (Rieger) dynamics of the solar wind. Per field component (panels a–c) and the total field (panel d and the same but smoothed in panel e). Note that results from the radial-field (panel a) and total-field (panels d–e) components are virtually the same, as expected due to a lack of significant density variations in Jupiter, and the heads-on (Sun-outward vs. Jupiter-outward) collision between the planetary magnetic field and the solar wind in the RTN coordinate system. One epoch spans one Earth year as an arbitrary and convenient field sampling size, except for the Cassini ("C–" label) case where the data extended over an eight-month interval, including an extra month respectively prepended and appended to the October 2000–March 2001 flyby and spanning 1 September 2000–30 April 2001 for that case. *Right composite*: a blind-plots stack of spectral-peak splitting due to anisotropy under magnetoactivity upsurge since 1996. Amplitudes not to scale. Note the 2001/2002 Cassini flyby case, where average spectra are seen as dominated by a single Rieger period due to a remote tangential flyby and its duration of half a year, so locking to one preferential frequency, which gave the impression of power absorption, was to be expected. The same preferential locking is in Juno ("J–") vs. Galileo ("G–") spectra due to Juno's highly varying altitude, including regular crossings of the magnetopause. Cassini data included an extra month to the October 2000–March 2001 flyby and thus spanned 1 September 2000–30 April 2001. Short-dashed line marks the 67%- significance level, with the 99%-level always nearby (long-dashed on radial-component plots for illustration). The Galileo and Juno data were magnetometer recordings provided by the UCLA–NASA data team, in batches as concatenated and rotated to RTN (Sun) coordinate frame (see Acknowledgments). See statements for information on the complete decimated data sets. Note that the frequency–magnitude blind spectral plots on the right-hand side are not intended for any rigorous considerations and are for illustration purposes only (of resolving the general level of anisotropy change per the same unit of time used to track changes in magnetoactivity, i.e., via changes in the annual mean spectral magnitude). The overall uncertainty is ±5% (on all values).
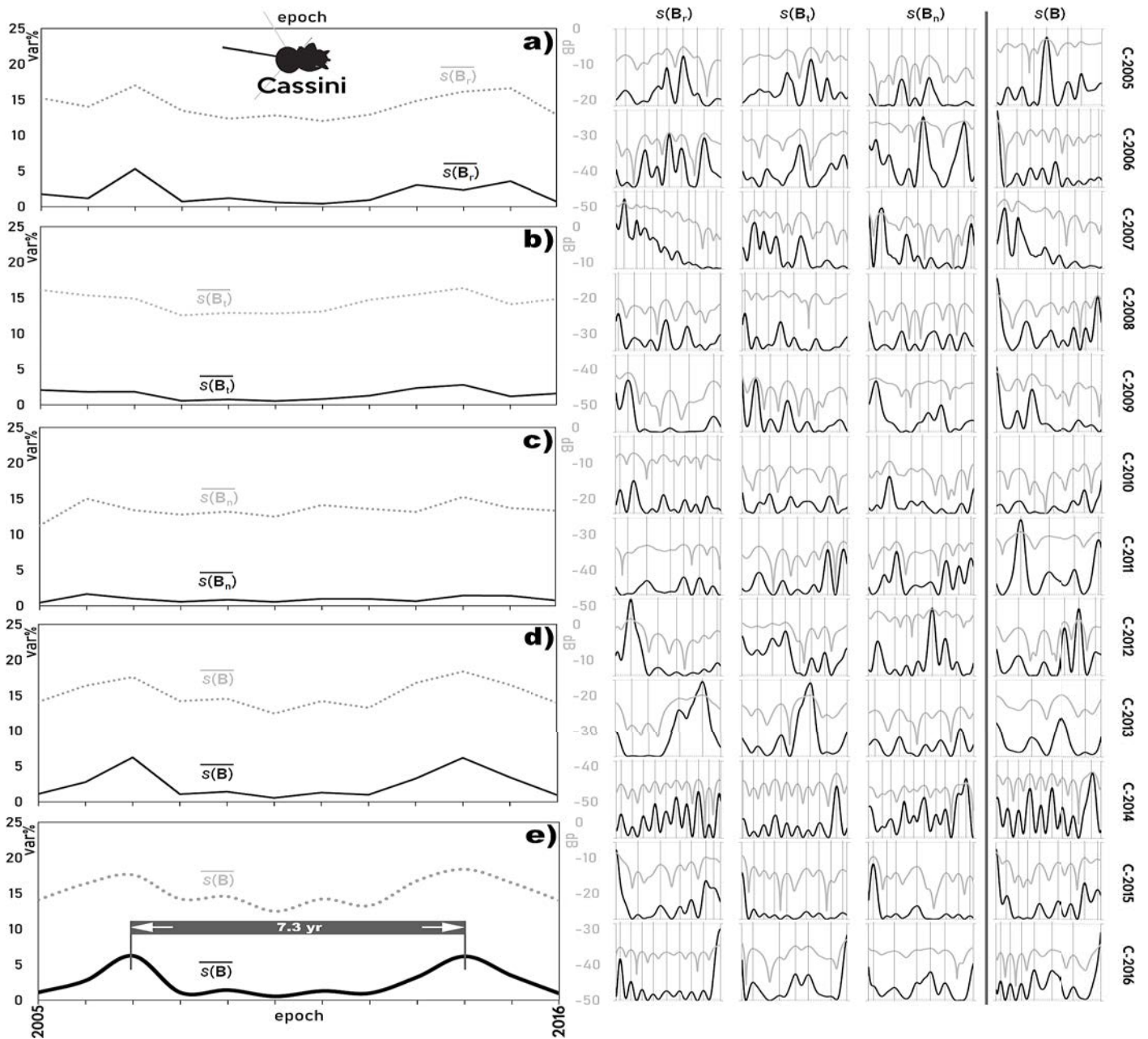
Figure 4. *Left composite*: Decade-scale relative change of Saturn magnetosphere activity with time as imprinted in the solar wind (IMF), as the change in mean GVSA spectral magnitudes in var% (solid black line) and dB (dotted gray) of annual Saturnian ⪅8nT global magnetic field in the 30–180-day band of most energetic (Rieger) dynamics of the solar wind. Per field component (panels a–c) and the total field (panel d and the same but smoothed in panel e). As in the Jupiter case (Fig. 3), results from the radial-field (panel a) and total-field (panels d & e) components are virtually the same, as expected due to a lack of significant density variations in Saturn, and the heads-on (Sun-outward vs. Saturn-outward) collision between the planetary magnetic field and the solar wind in the RTN coordinate system. Here Saturn's global magnetic field is seen as perhaps forced by a ~7.1-yr period, possibly its ¼T_{orbit}, $T_{orbit} \approx$ 29.4 years, orbital tide as transpired via the solar wind. One epoch spans one Earth year as an arbitrary and convenient field sampling size. *Right composite*: a blind-plots stack of spectral-peak splitting due to anisotropy. Unlike Jupiter, anisotropy in the Saturn magnetosphere shows no clear temporal trending overall, revealing random and very weak upsurges as seen from the number of split peaks per blind plot rarely exceeding eight (a degree of freedom beyond the set of seven Rieger periodicities). Amplitudes not to scale. Short-dashed line marks the 67%-significance level and practically coincides with the abscissa in all panels, with the 99%-level always nearby to within a few var% (shown long-dashed on radial-component plots for illustration). The data used were 2005–2016 Cassini magnetometer recordings (Dougherty et al., 2006). See statements for information on the complete decimated data set. The purpose of frequency–magnitude blind spectral plots (right-hand side) is as in Fig. 3. The overall uncertainty is ±5% (on all values).

12

4. Discussion

Jupiter magnetoactivity is both internally and solar-wind-driven (Vogt et al., 2019). Because interaction between the solar wind's highly variable external conditions and the (solar wind-shaped) magnetospheres is essential for understanding energy flow within a planetary system, the nature of the solar wind–Jupiter magnetosphere interaction has been widely debated but remains poorly understood (Masters, 2017). However, we know that such an interaction has been established even between the solar wind and Jupiter inner magnetosphere based on the Hisaki satellite observations (Murakami et al., 2016). Also, the solar wind can produce compressional mode waves in the magnetosphere (Cho et al., 2017), and Jupiter is sufficiently far away from the Sun to make the effect of the solar wind less serious (Fan et al., 1982). Therefore, and since the Jupiter magnetosphere is the most powerful planetary particle accelerator in our solar system (Saur et al., 2017) so the signatures of the solar wind in the magnetospheres are too faint, the present study then attempts to fill the void by extracting the opposite effect. Thus I set out to detect spectral signatures of the Jupiter magnetosphere's activity in the solar wind instead — by establishing if there is such an interaction for the wind's highest-energies dynamics. Because such an interaction is shown in the present study to apply in the frequency space (by way of the spectral magnitude space), the interaction's dominant periodicities likely drive numerous unexplained (but probably resonant) periodicities on Jupiter and Saturn, from subdiurnal to several days in duration. Namely, a clear ~26-day solar periodicity is seen in the Cassini data (Stallard et al., 2019), while solar wind-induced periodicities in the magnetosphere are ~13 or ~26 days (Roussos et al., 2018) as well as the Rieger-type and longer periodicities (Lou et al., 2003). In addition, Chancia et al. (2019) have noticed certain resonant features in the Saturn magnetosphere, with expected pattern speeds much slower than the magnetospheric periodicities.

Since ~2001, the evolution of Jupiter's decade-scale global magnetoactivity in the RR band took an increasingly sinusoidal form, Fig. 2, as well as Fig. 3 vs. Fig. 4, seen in magnetar 4U 0142+61. This mode of global tiredness in which a system dissipates energy in an increasingly sinusoidal manner is in astrophysics found not only in magnetars but other types of astronomical bodies as well. For example, superhumps or superoutbursts (long outbursts) are seen in dwarf novae when a non-sinusoidal pulse shape becomes increasingly sinusoidal as the amplitude declines (Kuznetsova et al., 1999). In geology, the above release regime is part of metasomatic metamorphism — a chemical transformation of rock due to fluid-induced reaction, e.g., Aulbach et al. (2018). Thus as cross-scale and cross-discipline, this mode of system energy dissipation via gradually increasing divergence from/into the sinusoidal form could be more common than previously thought.

GVSA, as a rigorous method of spectral analysis, was used here to extract resonance/turbulence processes, including anisotropic peak splitting, with a satisfying relative resolution, Figs. 3 & 4. Note that fidelity, as a GVSA tool for such extractions of wave packets, could not be used in the context of the main result (increasingly sinusoidal energy dissipation mode from mean spectra) also because Φ is a property of a single spectral peak, determined in relation to an adjacent spectral peak so that a "Φ of an average peak" has no physical meaning. Note also that noise was not modeled in the present study. For red noise to be present and detrimental, it would have to escape the P_{Rg} mismatch of the epoch window, noted before as on the safe side by a factor of 0.2 at least. Secondly, for red noise effects to become detrimental, P_{Rg} would have to be the only and always the strongest Rieger periodicity despite the power constantly shifting amongst Rieger harmonics due to the transient nature of the whole process, i.e., not just P_{Rg}. But even in the unlikely scenario of both of the above circumstances occurring most of the time, red noise would still be adding some relatively small systematics also systematically — to the epoch values of mean spectral magnitude, Fig. 3, i.e., so that the increasingly sinusoidal form of system energy dissipation, Fig. 3-d & e, would be preserved. As for geophysical/background

noise, its effects can be handled methodologically for pulsars, as seen in Dib et al. (2007) vis-à-vis Woods et al. (2004).

The demonstration of Jupiter's nature as a real pulsar is even more credible since it successfully extracted a well-known (albeit poorly understood) natural mode of system energy dissipation from 12+ billion combined-mission *in situ* measurements spanning a quarter of a century. The demonstration included a comparison against *in situ* measurements at Saturn as the only other similar body within our reach, taken within the same few decades. As Saturn is the most similar to Jupiter in our solar system, this similarity suffices for comparing the change in their global dynamics over the same few decades but is not of use for direct comparisons of their behavior from the same or different epochs (years). In addition, energy levels in Jupiter are stratified under rotation virtually radially so that all the effects from all types of noises — statistical of all colors and physical/local including background, contamination, whistler, and mixing — can be expected to cancel out over several months, and vanish entirely over decades as in this case. Besides, dynamics at the highest energies of a physical system are magnitudes of order above energy levels of any noise, even various noise types combined, so a mathematically rigorous treatment of noise here can be safely left out. Finally, since such noise treatments are redundant in pulsars, then by extension, those treatments would be expectedly irrelevant for the Jupiter case. Drawing this parallel is appropriate not only due to the aforementioned guiding role of rotation and the related cancelation of all noise effects over decades but also because of Jupiter's minute size/energy output relative to pulsars; see, e.g., Dowden (1968) for a physical model-comparison of those energy emission levels from pulsar vs. Jovian bursting.

In many ways, Jupiter behaves like a pulsar (Dowden, 1968) (Fan et al., 1982), so Jupiter is a very weak pulsar itself since Jupiter's both magnetic moment and angular momentum are only slightly less than in pulsars (Michel, 1982). Similarly, as indicators of planetary magnetoactivity, ion aurorae share common mechanisms across planetary systems, despite temporal, spatial, and energetic scales varying by orders of magnitude (Yao et al., 2021). Since we can expect all macroscale (especially astrophysical) magnetic fields to behave in such ways regardless of scale, the above conclusions probably hold for magnetars as well. Magnetars are young isolated neutron stars characterized by exceptionally high X-ray luminosity and are extremely rare, so only about 20 active such objects are currently known in the observable universe. They are discovered either by analyzing their steady X-ray emission or in outburst events, but in both cases, they supply most energy from the decay and instabilities of very intense magnetic fields of $\gtrsim 10^{14}$ G (Pizzocaro et al., 2019). As such, magnetars act overwhelmingly on all other forces in their vicinity, making them natural laboratories for observing and learning about general processes and mechanisms of astrophysical magnetic fields under the most extreme conditions that can create nearly perfect isolation.

To study high-energy bursts from magnetars as remote astronomical objects for which detailed magnetic field measurements are thus unavailable, astronomers rely not only on observations of proxies such as X-ray emissions but also on changes in persistent emissions, as well as spectra of surface or internal processes and instabilities. On the other hand, the Jupiter magnetosphere is within our reach and has been sampled directly in nearly a dozen Space missions. So the main result of the present study — the evolution profile of the decade-scale global planetary magnetoactivity shown in Fig. 3 — has been obtained from all available ≥6 months-long *in situ* measurements of the Jovian magnetic field. Given that the energy scales involved are the highest possible for that planet, the result conclusively showed that Jupiter's magnetoactivity presently is the highest possible and that much of this activity gets naturally relayed via reconnecting to the surrounding environment. For instance, Sun-like stars with planetary systems expectedly erupt with superflares (Schaefer et al., 2000).

While Jupiter-like gaseous giants in close orbits about Sun-like stars could theoretically cause such events, apparently Jupiter is too remote from the Sun to be capable of

causing solar superflares via magnetic tangling under reconnecting (Rubenstein and Schaefer, 2000). However, the physics of such magnetic reconnecting is mainly unknown (*ibid*.). Therefore, a Jupiter-like giant with its own flaring mechanism (regardless if capable of flaring palpably or not), especially in cases of purely magnetic and rotational such mechanism like Jupiter's, could perhaps also entangle its primary star's magnetic field on decadal scales without causing observable rotational variations in the host star or extinction-level superflares. Namely, such superflares could not be linked to mass extinctions in the geological record (*ibid*.).

A conventional but *ad hoc* criterion for defining a planet as a brown dwarf is that the planetary mass must exceed $13.6M_{Jupiter}$. Another criterion, which has support of an important fraction of the astronomical community, is based on the origins of the object's formation instead (Chauvin et al., 2005). While the difference between a relatively high-mass gaseous planet like Jupiter and a low-mass brown dwarf is still a matter of debate, it is rather unfortunate that neither of the above most vocal schools of thought (scale-based and internal-physics-based criteria vs. way-of-formation criteria) advocates external physics, i.e., current activity or lack of it, as the criterion. Just as gaseous giant planets often get termed *failed stars* for their inability to sufficiently amass and ignite a core early on in their history, Jupiter too is termed *a failed brown dwarf* (Fukuhara, 2020). However, those objects have not entirely failed if their physical or chemical properties amount to star-like global activity sufficient to act on active (fusing) stars. So based on its activity type and extent rather than purely scale-based (therefore arbitrary) conventional criteria like mass or distance from the primary star, Jupiter meets *natural criteria* to be re-classified to a pulsar. Namely, as shown in the present study, it behaves under its rotation like any magnetar pulsar; and whether it could affect its primary star just like a dwarf star in binary stellar systems can is an open question. Importantly, planetary-mass brown dwarfs have been observed (Luhman et al., 2005).

The Rieger process involves the heliosphere proper (and thus the IMF) with planets — of which gaseous giants probably are most significant due to vast magnetospheres. Because Jupiters in other stellar systems affect host stars dynamically, e.g., by causing stars to pulsate harmonically at multiples of the planet's orbital frequency (de Witt et al., 2017), Jupiter could hypothetically also affect the Sun in the frequency space. And given that (only) the Jovian magnetosphere extends to other planets, then by extension, Jupiter could affect other planets in between as well, like Mars and Earth. In addition, the Jovian magnetic field is currently undergoing a polarity reversal (Grote and Busse, 2000) or a transition between different dynamo states (Duarte et al., 2018), as implied by the Juno mission (Moore et al., 2018). But even before the Juno mission became operational, Pap et al. (1990) offered an intuitive yet analogous explanation, proposing that the existence of the transient 154±13-day Rieger period was related to an emerging strong magnetic field.

While the primary source of magnetospheric power for Jupiter is the planet's spin, the present study has confirmed that a spinning planetary magnetic field interacts with plasma in solar wind's lowermost frequencies (here: the most significant alternative plasma source to the Jovian moon Io). This interaction and others could provide energy for global (dipoleside) bursts by creating a torque that slows the Jupiter rotation, thus providing power for an entire variety of magnetospheric phenomena to occur (Dessler, 1987). Then a global outburst of dipolar beam ejecta of pulsar type is one such plausible event.

Because the present global data-based study was successful in extracting the pulsar behavior of Jupiter on decadal scales, its results are unlikely to lend themselves to any magnetohydrodynamics (MHD) theory (Alfvén, 1942) considerations since MHD is an approximation theory inapplicable to magnetospheres of pulsars (Spruit, 2017). Thus stellar global properties, as used in the present study, such as the suggested magnetic tangling, are not necessarily the same processes or tangling as understood or speculated classically within the framework of MHD.

15

5. Conclusions

The present study conclusively-computationally and for the first time confirmed the long-suspected pulsar nature of Jupiter, which turns out to be not just a low-power pulsar analog at the spin period of the planet as believed previously — but a high-power pulsar of magnetar-novae type. Specifically, the magnetoactivity evolution profile of the 4U 0142+61 magnetar, preceding its short-burst high-energy pulsations, and whose decadal-scale preparation phase had been extracted previously from highest-resolution data, is comparable to the magnetoactivity evolution profile of Jupiter and possible (as-of-yet un-observed) high-energy global outbursts of pulsar type. Then the Jupiter magnetoactivity increase — revealed here by the decadal-scale global activity such profile from mean spectra of annual magnetometer records obtained by integrating Galileo, Cassini, and Juno data — is the highest possible in a planetary magnetosphere in our solar system. While this multi-mission and multi-planetary study has demonstrated that Jupiter currently exhibits magnetar- and dwarf novae-type pre-bursting pulsating behavior on decadal scales, also shared by some physicochemical systems in Nature, the level of danger this behavior poses is presently unknown. However, the uniqueness of the approach — which has utilized 12+ billion (all available) *in situ* data — makes this outcome the best we can do presently. Moreover, this demonstration of Jupiter as a sub-brown dwarf star of pulsar type that exhibits global behavior observed in objects that burst out regularly on decadal scales has implications for studying and modeling star creation and collapse. In addition, GVSA variance-spectral magnitudes of the planetary magnetosphere–solar wind interaction rates, controlled in the band of highest planetary energies by the well-known (but little studied) Rieger resonant process of the wind's macroscopic dynamics, turned out to be a novel and practical proxy-gauge of global relative dynamics of astronomical bodies.

In summary, the present reproducible computational study based on billions of data from all three space missions that collected magnetometer measurements at Jupiter for six months or longer has revealed a previously reported cross-scale, gradually varying sinusoidal mode of systematic global decadal planetary dynamics that reached and maintained a staggering 20%+ field variance level. Generally, this mode of gradual global energy fluctuation can be said to describe how Jupiters jump between the star and planet states. Not only does a discovery under such a set of most important (concerning highest energy levels in the studied astronomical body) circumstances alone confirm the associated computations as correct, but the result subsequently got confirmed in absolute terms as well — against global decade-scale magnetodynamics of Saturn as the only other similar planet with also *in situ* data. Any study in the energy band of global planetary (closed physical system) dynamics that reproduces a previously reported regular dynamic is beyond doubt correct ("by definition") and overrides, redefines, and completes all considerations at lower energy levels at once, including those in disagreement with the result. By extension, questions about not utilizing the competing spectral analysis methodology for comparison or about averaging multi-mission data without considering possible orbital modulation effects become moot points.

The present study exposed the critical possibility of Jupiter's outbursting capacity. Such an outcome demands the broadest efforts toward learning more about the threats from Jovian global high-energy outbursts. Such all-bursts, found here capable of dissipating up to ~20% of the total planetary magnetic field energy, could take on the form of magnetopolar beams alongside the dipole under the 10º tilt (up to 13º to the ecliptic with obliquity). Those energetic beams would pose an immediate danger, primarily to solar-system space missions and communications infrastructure, but also to planetary power grids and installations. This scenario then calls for the deployment of permanent multi-vessel missions for real-time monitoring of the magnetoactivity of pulsar Jupiter.

Data Access Statement: The Saturn original magnetometer RTN data underlying this article are publicly available at https://pds-atmospheres.nmsu.edu/data_and_services/atmospheres_data/Cassini. The Jupiter original magnetometer data concatenated and rotated to RTN coordinate frame may be available from UCLA & NASA PPI upon request (see Acknowledgments). Decimated data sets, as used to obtain the main results shown in Figs. 2–4 and throughout the present study are in a Supplement accompanying this manuscript, which can be obtained from a repository at https://dx.doi.org/10.21227/bs6p-5456.

Declaration of interest: The author declares no conflict of interest.

References

Alfvén, H. (1942) Existence of electromagnetic-hydrodynamic waves. *Nature* 150(3805):405–406. https://doi.org/10.1038%2F150405d0

Aulbach, S., Heaman, L.M., Stachel, T. (2018) *The Diamondiferous Mantle Root Beneath the Central Slave Craton*. Geoscience and Exploration of the Argyle, Bunder, Diavik, and Murowa Diamond Deposits. ISBN 9781629496399. https://doi.org/10.5382/SP.20.15

Bai T. and Cliver E. W. (1990) A 154 day periodicity in the occurrence rate of proton flares. *Astrophys. J.* 363:299–309. https://doi.org/10.1086/169342

Cane, H.V., Richardson, I.G., von Rosenvinge, T.T. (1998) Interplanetary magnetic field periodicity of ~153 days. *Geophys. Res. Lett.* 25(24):4437–4440. https://doi.org/10.1029/1998GL900208

Carbonell, M., Ballester, J.L. (1992) The periodic behaviour of solar activity – The near 155-day periodicity in sunspot areas. *Astron. Astrophys.* 255(1–2):350–362. https://ui.adsabs.harvard.edu/#abs/1992A&A...255..350C

Chancia, R.O., Hedman, M.M., Cowley, S.W.H., Provan, G., Ye, S.–Y. (2019) Seasonal structures in Saturn's dusty Roche Division correspond to periodicities of the planet's magnetosphere. *Icarus* 330:230–255. https://doi.org/10.1016/j.icarus.2019.04.012

Chauvin, G., Lagrange, A.–M., Zuckerman, B., Dumas, C., Mouillet, D., Song, I., Beuzit, J.–L., Lowrance, P., Bessell, M.S. (2005) A companion to AB Pic at the planet/brown dwarf boundary. *Astron. Astrophys.* 438(3):L29–L32. https://doi.org/10.1051/0004-6361:200500111

Cho, J.–H., Lee, D.–Y., Noh, S.–J., Kim, H., Choi, C.R., Lee, J., Hwang, J., (2017) Spatial dependence of electromagnetic ion cyclotron waves triggered by solar wind dynamic pressure enhancements. *J. Geophys. Res. Space Phys.* 122, 5502–5518. https://doi.org/10.1002/2016JA023827

Chowdhury, P., Khan, M., Ray, P.C. (2009) Intermediate-term periodicities in sunspot areas during solar cycles 22 and 23. *Mon. Not. R. Astron. Soc.* 392(1):1159–1180. https://doi.org/10.1111/j.1365-2966.2008.14117.x

Craymer, M.R. (1998) *The Least Squares Spectrum, Its Inverse Transform and Autocorrelation Function: Theory and Some Applications in Geodesy*. Ph.D. Dissertation, University of Toronto, Canada. https://hdl.handle.net/1807/12263

Dessler, A.J. (1987) *Magnetospheric power from planetary spin* (p.71). IEEE international conference on plasma science, 1–3 June, Crystal City, VA USA

Dib, R., Kaspi, V.M., Gavriil, F.P. (2007) 10 Years of RXTE monitoring of the anomalous X-ray pulsar 4U 0142+61: long-term variability. *Astrophys. J.* 666(2):1152-1164. https://doi.org/10.1086/519726

Dimitropoulou, M., Moussas, X., Strintzi, D. (2008) Enhanced Rieger type periodicities' detection in X-ray solar flares and statistical validation of Rossby waves' existence. *Proc. Int. Astron. Union* 4(S257):159–163. https://doi.org/10.1017/S1743921309029226

Dougherty, M.K., Kellock, S., Slootweg, A.P., Achilleos, N., Joy, S.P., Mafi, J.N. (2006) *Cassini orbiter magnetometer calibrated 1 minute averaged archive v2.0 & v.1.0, CO-E/SW/J/S-MAG-4-SUMM-AVG1MIN-V2.0*. NASA Planetary Data System. https://doi.org/10.17189/1519602

Dowden, R.L. (1968) A Jupiter Model of Pulsars. *Pubs. Astron. Soc. Austral.* 1(4):159–159. https://doi.org/10.1017/s132335800001122x

Duarte, L.D.V., Wicht, J., Gastinec, T. (2018) Physical conditions for Jupiter-like dynamo models. *Icarus* 299:206–221. https://doi.org/10.1016/j.icarus.2017.07.016

Fan, C.Y., Wu, J., Hang, H. (1982) Scaling from Jupiter to pulsars and mass spectrum of pulsars. *Astrophys. J.* 260(1):353–361. https://ui.adsabs.harvard.edu/abs/1982ApJ...260..353F

Fukuhara, M. (2020) Possible nuclear fusion of deuteron in the cores of Earth, Jupiter, Saturn, and brown dwarfs. *AIP Advances* 10:035126. https://doi.org/10.1063/1.5108922

Ge, Y.S., Jian, L.K., Russell, C.T. (2007) Growth phase of Jovian substorms. *Geophys. Res. Lett.* 34:L23106. https://doi.org/10.1029/2007GL031987

Gaulme, P., Schmider, F.-X., Gay, J., Guillot, T., Jacob, C. (2011) Detection of Jovian seismic waves: a new probe of its interior structure. *Astron. Astrophys.* 531:A104. https://doi.org/10.1051/0004-6361/201116903

Gonzalez, M.E., Dib, R., Kaspi, V.M., Woods, P.M., Tam, C.R., Gavriil, F.P. (2010) Long-term X-ray changes in the emission from the anomalous X-ray pulsar 4U 0142+61. *Astrophys. J.* 716:1345–1355. https://dx.doi.org/10.1088/0004-637X/716/2/1345

Grote, E., Busse, F.H. (2000) Hemispherical dynamos generated by convection in rotating spherical shells. *Phys. Rev. E* 62:4457–4460. https://doi.org/10.1103/PhysRevE.62.4457

Kinkhabwala, A. (2013) *Maximum Fidelity*. Max Planck Institute of Molecular Physiology report. *arXiv*:1301.5186, Subject: Statistics Theory (math.ST). https://doi.org/10.48550/arXiv.1301.5186

Kiplinger, A.L., Dennis, B.R., Orwig, L.E. (1984) Detection of a 158 Day Periodicity in the Solar Hard X-Ray Flare Rate. *Bull. Amer. Astron. Soc.* 16:891. https://ui.adsabs.harvard.edu/#abs/1984BAAS...16..891K

Kuznetsova, Yu.G., Pavlenko, E.P., Sharipova, L.M., Shugarov, S.Yu. (1999) Observations of Typical, Rare and Unique Phenomena in Close Binaries with Extremal Mass Ratio. *Odessa Astron. Pub.* 12:197–200. https://ui.adsabs.harvard.edu/#abs/1999OAP....12..197K

Lou, Y.–Q., Wang, Y.–M., Fan, Z., Wang, S., Wang, J.X. (2003) Periodicities in solar coronal mass ejections. *Mon. Not. R. Astron. Soc.* 345(3):809–818. https://doi.org/10.1046/j.1365-8711.2003.06993.x

Luhman, K.L., Adame, L., D'Alessio, P., Calvet, N., Hartmann, L., Megeath, S.T., Fazio, G.G. (2005) Discovery of a planetary-mass brown dwarf with a circumstellar disk. *Astrophys. J.* 635(1):L93. https://doi.org/10.1086/498868

Manners, H., Masters, A. (2020) The global distribution of ultralow-frequency waves in Jupiter's magnetosphere. *J. Geophys. Res. Space Phys.* 125:e2020JA028345. https://doi.org/10.1029/2020JA028345

Masters, M. (2017) *Revealing how the solar wind interacts with Jupiter's magnetosphere*. Magnetospheres of the outer planets (MOP), Conference by the Swedish Institute for Space Physics & Royal Institute of Technology, Uppsala 12–16 Jun.

Matsushita S. (1967) Solar quiet and lunar daily variation fields. In: Matsushita S. Campbell W.H. (Eds.) *Physics of Geomagnetic Phenomena: International Geophysics Series, Vol. 2*, p. 301–424. Academic Press Inc., New York. Reprint 2016, Elsevier. ISBN 9781483222523. https://doi.org/10.1016/B978-0-12-480301-5.50013-6

Michel, F.C. (1982) Theory of pulsar magnetospheres. *Rev. Mod. Phys.* 54:1. https://doi.org/10.1103/RevModPhys.54.1

Moore, K.M., Yadav, R.K., Kulowski, L., Cao, H., Bloxham, J., Connerney, J.E.P., Kotsiaros, S., Jørgensen, J.L., Merayo, J.M.G., Stevenson, D.J., Bolton, S.J., Levin, S.M. (2018) A complex dynamo inferred from the hemispheric dichotomy of Jupiter's magnetic field. *Nature* 561:76–78. https://doi.org/10.1038/s41586-018-0468-5

Murakami, G., Yoshioka, K., Yamazaki, A., Tsuchiya, F., Kimura, T., Tao, C., Kita, H., Kagitani, M., Sakanoi, T., Uemizu, K., Kasaba, Y., Yoshikawa, I., Fujimoto, M. (2016) Response of Jupiter's inner magnetosphere to the solar wind derived from extreme ultraviolet monitoring of the Io plasma torus. *Geophys. Res. Lett.* 43:12308–12316. https://doi.org/10.1002/2016GL071675

von Neumann, J. (1941) Distribution of the Ratio of the Mean Square Successive Difference to the Variance. *Ann. Math. Statist.* 12(4):367–395. https://doi.org/10.1214/aoms/1177731677

Omerbashich, M. (2023a) First total recovery of Sun global Alfven resonance: least-squares spectra of decade-scale dynamics of N-S-separated fast solar wind reveal solar-type stars act as revolving-field magnetoalternators. *arXiv*:2301.07219, Subject: Solar and Stellar Astrophysics (astro-ph.SR). https://arxiv.org/abs/2301.07219

Omerbashich, M. (2023b) Sun resonant forcing of Mars, Moon, and Earth seismicity. *arXiv*:2301.10800, Subject: Earth and Planetary Astrophysics (astro-ph.EP). https://doi.org/10.48550/arXiv.2301.10800

Omerbashich, M. (2023c) Earth as a time crystal: macroscopic nature of a quantum-scale phenomenon from transformative moderation of geomagnetic polarity, topography, and climate by precession resonance due to many-body entrainment. *arXiv*:2301.02578, Subject: Geophysics (physics.geo-ph). https://doi.org/10.48550/arXiv.2301.02578

Omerbashich, M. (2021) Non-marine tetrapod extinctions solve extinction periodicity mystery. *Hist. Biol.* 34(1):188-191. https://doi.org/10.1080/08912963.2021.1907367

Omerbashich, M. (2020) Moon body resonance. *J. Geophys.* 63:30–42. https://n2t.net/ark:/88439/x034508

Omerbashich, M. (2009) *Method for Measuring Field Dynamics*. US Patent #20090192741, US Patent & Trademark Office. https://worldwide.espacenet.com/publicationDetails/biblio?CC=US&NR=2009192741A1

Omerbashich, M. (2007) Magnification of mantle resonance as a cause of tectonics. *Geodinamica Acta* 20:6:369–383. https://doi.org/10.3166/ga.20.369-383

Omerbashich, M. (2006) Gauss–Vaníček Spectral Analysis of the Sepkoski Compendium: No New Life Cycles. *Comp. Sci. Eng.* 8(4):26–30. https://doi.org/10.1109/MCSE.2006.68 (Erratum due to journal error. *Comp. Sci. Eng.* 9(4):5–6. https://doi.org/10.1109/MCSE.2007.79; full text: https://doi.org/10.48550/arXiv.math-ph/0608014)

Omerbashich, M. (2004) *Earth-model Discrimination Method*. Ph.D. Dissertation, pp.129. ProQuest, USA. https://doi.org/10.6084/m9.figshare.12847304

Pagiatakis, S. (1999) Stochastic significance of peaks in the least-squares spectrum. *J. Geod.* 73:67–78. https://doi.org/10.1007/s001900050220

Pap, J., Tobiska, W.K., Bouwer, S.D. (1990) Periodicities of solar irradiance and solar activity indices, I. *Sol. Phys.* 129:165–189. https://doi.org/10.1007/BF00154372

Pizzocaro, D., Tiengo, A., Mereghetti, S., Turolla, R., Esposito, P., Stella, L., Zane, S., Rea, N., Coti Zelati, F., Israel, G. (2019) Detailed X-ray spectroscopy of the magnetar 1E 2259+586. *Astron. Astrophys.* 626:A39. https://doi.org/10.1051/0004-6361/201834784

Press, W.H., Teukolsky, S.A., Vetterling, W.T., Flannery, B.P. (2007) *Numerical Recipes: The Art of Scientific Computing* (3rd Ed.). Cambridge University Press, United Kingdom. ISBN 9780521880688

Rieger, E., Share, G.H., Forrest, D.J., Kanbach, G., Reppin, C., Chupp, E.L. (1984) A 154-day periodicity in the occurrence of hard solar flares? *Nature* 312:623–625. https://doi.org/10.1038/312623a0

Roussos, E., Krupp, N., Paranicas, C., Kollmann, P., Mitchell, D.G., Krimigis, S.M., Palmaerts, B., Dialynas, K., Jackman, C.M. (2018) Heliospheric conditions at Saturn during Cassini's ring-grazing and proximal orbits. *Geophys. Res. Lett.* 45:10812–10818. https://doi.org/10.1029/2018GL078093

Rubenstein, E.P., Schaefer, B.E. (2000) Are Superflares on Solar Analogues Caused by Extrasolar Planets? *Astrophys. J.* 529(2):1031. https://doi.org/10.1086/308326

Saur, J., Schreiner, A., Mauk, B.H., Clark, G.B., Kollmann, P. (2017) *Wave particle interactions in Jupiter's magnetosphere and associated particle acceleration*. Magnetospheres of the outer planets (MOP), Conference by the Swedish Institute for Space Physics and Royal Institute of Technology, Uppsala Sweden, 12–16 June.

Schaefer, B.E., King, J.R., Deliyannis, C.P. (2000) Superflares on ordinary solar-type stars. *Astrophys. J.* 529(2):1026. https://doi.org/10.1086/308325

Shannon, C.E. (1948) A Mathematical Theory of Communication. *Bell System Tech. J.* 27:379–423, 623–656. https://doi.org/10.1002/j.1538-7305.1948.tb01338.x

Spruit, H.C. (2017) *Essential magnetohydrodynamics for astrophysics*. An introduction to magnetohydrodynamics in astrophysics. A report by Max Planck Institute for Astrophysics. *arXiv*:1301.5572, Subject: Instrumentation & Methods for Astrophysics (astro-ph.IM). https://doi.org/10.48550/arXiv.1301.5572

Stallard, T.S., Baines, K.H., Melin, H., Bradley, T.J., Moore, L., O'Donoghue, J., Miller, S., Chowdhury, M.N., Badman, S.V., Allison, H.J., Roussos, E. (2019) Local-time averaged maps of H3$^+$ emission, temperature and ion winds. *Phil. Trans. R. Soc. A.* 3772018040520180405. https://doi.org/10.1098/rsta.2018.0405

Steeves, R.R. (1981). *A statistical test for significance of peaks in the least squares spectrum*. Collected Papers, Geodetic Survey, Department of Energy, Mines and Resources. Surveys and Mapping Branch, Ottawa Canada, pp. 149–166. http://www2.unb.ca/gge/Research/GRL/LSSA/Literature/Steeves1981.pdf

Taylor, J., Hamilton, S. (1972) Some tests of the Vaníček Method of spectral analysis. *Astrophys. Space Sci.* 17:357–367. https://doi.org/10.1007/BF00642907

Tsuchiya, F., Yoshioka, K., Kimura, T., Koga, R., Murakami, G., Yamazaki, A., Kagitani, M., Tao, C., Suzuki, F., Hikida, R., Yoshikawa, I., Kasaba, Y., Kita, H., Misawa, H., Sakanoi, T. (2018) Enhancement of the Jovian magnetospheric plasma circulation caused by the change in plasma supply from the satellite Io. *J. Geophys. Res. Space Phys.* 123:6514–6532. https://doi.org/10.1029/2018JA025316

Vaníček, P. (1969) Approximate spectral analysis by least-squares fit. *Astrophys. Space Sci.* 4(4):387–391. https://doi.org/10.1007/BF00651344

Vaníček, P. (1971) Further development and properties of the spectral analysis by least-squares fit. *Astrophys. Space Sci.* 12(1):10–33. https://doi.org/10.1007/BF00656134

Vogt, M.F., Gyalay, S., Kronberg, E.A., Bunce, E.J., Kurth, W.S., Zieger, B., Tao, C. (2019) Solar Wind Interaction With Jupiter's Magnetosphere: A Statistical Study of Galileo In Situ Data and Modeled Upstream Solar Wind Conditions. *J. Geophys. Res. Space Phys.* 124(12):10170–10199. https://doi.org/10.1029/2019JA026950

Wells, D.E., Vaníček, P., Pagiatakis, S. (1985) *Least squares spectral analysis revisited*. Department of Geodesy & Geomatics Engineering Technical Report 84, University of New Brunswick, Canada. http://www2.unb.ca/gge/Pubs/TR84.pdf

de Wit, J., Lewis, N.K., Knutson, H.A., Fuller, J., Antoci, V., Fulton, B.J., Laughlin, G., Deming, D., Shporer, A., Batygin, K. (2017) Planet-induced Stellar Pulsations in HAT-P-2's Eccentric System. *Astrophys. J. Lett.* 836(2):L17. https://doi.org/10.3847/2041-8213/836/2/L17

Woods, P.M., Kaspi, V.M., Thompson, C., Gavriil, F.P., Marshall, H.L., Chakrabarty, D., Flanagan, K., Heyl, J., Hernquist, L. (2004) Changes in the X-Ray emission from the magnetar candidate 1E 2259+586 during its 2002 outburst. *Astrophys. J.* 605(1):378-399. https://doi.org/10.1086/382233

Wright, A.N., Mann, I.R. (2013) Global MHD eigenmodes of the outer magnetosphere. In Magnetospheric ULF Waves: Synthesis and New Directions. *Geophys. Monogr. Ser.* 169, pp. 51–72. https://doi.org/10.1029/169GM06

Yao, Z., Dunn, W.R., Woodfield, E.E., Clark, G., Mauk, B.H. et al. (2021) Revealing the source of Jupiter's x-ray auroral flares. *Sci. Adv.* 7:eabf0851. https://doi.org/10.1126/sciadv.abf0851

Zhou, W.X., Sornette, D. (2002) Statistical significance of periodicity and log-periodicity with heavy-tailed correlated noise. *Int. J. Mod. Phys.* 13(2):137-169. https://doi.org/10.1142/S0129183102003024